Effective Spin Foam Models for Four-Dimensional Quantum Gravity

Seth K. Asante,[1,2] Bianca Dittrich,[1] and Hal M. Haggard[3,1,*]

[1]Perimeter Institute, 31 Caroline Street North, Waterloo, Ontario N2L 2Y5, Canada
[2]Department of Physics and Astronomy, University of Waterloo, 200 University Avenue West, Waterloo, Ontario N2L 3G1, Canada
[3]Physics Program, Bard College, 30 Campus Road, Annandale-On-Hudson, New York 12504, USA

(Received 28 April 2020; revised 3 August 2020; accepted 10 November 2020; published 1 December 2020)

A number of approaches to four-dimensional quantum gravity, such as loop quantum gravity and holography, situate areas as their fundamental variables. However, this choice of kinematics can easily lead to gravitational dynamics peaked on flat spacetimes. We show that this is due to how regions are glued in the gravitational path integral via a discrete spin foam model. We introduce a family of "effective" spin foam models that incorporate a quantum area spectrum, impose gluing constraints as strongly as possible, and leverage the discrete general relativity action to specify amplitudes. These effective spin foam models avoid flatness in a restricted regime of the parameter space.

DOI: 10.1103/PhysRevLett.125.231301

Symplectic, metrical quantization.—Envisioning the geometry of spacetime as dynamically evolving founded the revolutionary insights of general relativity (GR) that have resulted in direct measurements of gravitational time dilation, bending of starlight, and gravitational waves. However, this revolution remains incomplete. We still do not know how to fully characterize an evolving quantum spacetime geometry.

The quantization of spacetime geometry is an interplay between its symplectic and metrical aspects. The former determines the allowed phase space and its associated quantum theory, while the latter encodes spacetime dynamics. In three dimensions, alignment between these two facets of geometry allows one to construct a discrete, simplicial path integral for quantum gravity, the Ponzano-Regge model [1]. Spacetime is decomposed into a large collection of tetrahedra that are glued along a subset of edges with matched lengths. Metrical and symplectic aspects of this geometry nicely align: lengths encode the intrinsic metric and tetrahedral dihedral angles encode the extrinsic geometry, and these variables are canonically conjugated to each other [2,3]. In the Euclidean signature case, the angles are compact, which leads to discrete spectra for the lengths.

In four dimensions, the situation is more subtle, and there is some tension between the symplectic and the metrical. In a spacetime split, the metric has two natural discretizations: the lengths of edges and the extrinsic curvature angles defined around two dimensional (2D) faces.

These variables are not canonically conjugate. This forces a choice: either the lengths or the extrinsic curvature angles must be completed to a set of canonically conjugated coordinates.

If the lengths are chosen, then the conjugate variables are contractions of the curvature angles with certain area-length derivatives [4]. These variables have, so far, resisted rigorous quantization. Meanwhile for the curvature angles, the conjugate variables are the 2D face areas, whose quantization gives a discrete area spectrum; this is because they are conjugate to compact angles. These variables arise naturally in connection formulations of GR, like loop quantum gravity (LQG) [5]. A key result of LQG is the rigorous quantization of area and volume observables, which, indeed, have discrete spectra [6–9].

In spin foam models [10–12], which are discrete geometry path integrals derived from LQG, area variables are fundamental. Area variables play a central role in holography [13,14], in particular, for the reconstruction of geometry from entanglement [15,16], and discrete area spectra are key in many approaches to black hole entropy counting [17–20]. There is, however, an interplay between the choice of area variables and the dynamics of GR: in this Letter, we show that area variables must be constrained to avoid a suppression of curvature and that the discreteness of their spectra hinders sharp imposition of these constraints.

In fact, it has been argued that, in the semiclassical limit, flat configurations dominate the spin foam path integral [21–27]. We reveal the mechanism behind this unfortunate dominance and identify a more favorable regime in which the path integral can peak on curved configurations. This "flatness problem" has been a key open problem for spin foams [27]. We show that it can be traced back to fundamental, discrete, area variables.

We directly tackle the question of whether a discrete, locally independent, area spectrum is consistent with the dynamics of GR. To this end, we propose a family of "effective" models that (a) incorporate a discrete area spectrum, (b) impose the constraints between the areas as strongly as allowed by the LQG Hilbert space structure, and (c) use—more directly than current spin foam models—a discretized GR action for the amplitudes.

 © 2020 American Physical Society

These effective models allow us to show that the flatness problem can be overcome, but to do so also imposes certain restrictions involving the discretization scale, curvature per triangle, and the Barbero-Immirzi parameter, which controls the area spectral spacing. Future work will show whether these restrictions are sufficient to ensure general relativistic dynamics in the continuum limit.

Discrete, locally independent areas.—We study a path integral for 4D quantum gravity regulated by a triangulation of spacetime. We work with quantum amplitudes in Euclidean signature, leaving the Lorentzian case to future work. Our key assumption is that the areas have a discrete, prescribed spectrum. We take the area eigenvalues to be independent, that is, their values will not depend on the state away from the measured triangle. The particular area spectrum we work with is

$$a(j) = \gamma \ell_P^2 \sqrt{j(j+1)} \sim \gamma \ell_P^2 (j + 1/2), \tag{1}$$

where j is a half-integer spin label, $\ell_P = \sqrt{8\pi\hbar G/c^3}$ is the Planck length, γ is the dimensionless Barbero-Immirzi parameter, and $\sim$ indicates the large-j asymptotic limit. We focus on the equispaced asymptotic spectrum. This form for the area spectrum was established in LQG [6–9], but discrete areas have also been discussed in the context of black hole spectroscopy [17]. In LQG, triangle normals are represented by angular momentum vector operators rescaled by γ [28,29]. Thus, the area is given by the square root of the SU(2) Casimir, multiplied by γ, which determines the area eigenvalue spacing.

Before taking up the path integral, we review the use of area variables in simplicial discretizations of GR. These discretizations were introduced by Regge [30] and used length variables. A wide array of reformulations have been considered [31–36], and we use descriptive adjectives to capture the variables used in each form. The change from length to area variables turns out to be more subtle than one might expect. A treatment in the more transparent context of Regge calculus will illuminate the issues before discussing the path integral.

Actions for discretized GR.—In length Regge calculus (LRC), one replaces the metric by lengths l_e assigned to the edges e of a triangulation. The l_e determine the triangle areas $A_t(l)$, and the 4D (internal) dihedral angles $\theta_t^\sigma(l)$ in each four-simplex σ. The action

$$S_{\mathrm{LRC}} = \sum_t n_t \pi A_t - \sum_\sigma \sum_{t \supset \sigma} A_t \theta_t^\sigma \equiv \sum_t S_t^l + \sum_\sigma S_\sigma^l, \tag{2}$$

is a discretization of the Einstein-Hilbert action, and the corresponding equations of motion approximate Einstein's equations [37]. The factor $n_t \in \{1, 2\}$ allows for triangulations with boundary and is one for triangles on the boundary and two for triangles in the bulk.

The four-simplices, which are the basic building blocks of the triangulation, each have ten edges and ten areas. Thus, one can (locally) invert the ten functions $A_t(l)$ that give a simplex's areas in terms of its lengths [38]. We will denote the resulting functions $L_e^\sigma(a)$, where a collectively signifies the ten areas associated to σ. This allows us to define the area Regge calculus (ARC) action [31,32,36], whose value on configurations with $a_t = A_t(l)$ agrees with the LRC action

$$S_{\mathrm{ARC}} = \sum_t S_t^a(a) + \sum_\sigma S_\sigma^a(a), \tag{3}$$

where $S_t^a(a) = n_t \pi a_t$ and $S_\sigma^a(a) = S_\sigma^l[L^\sigma(a)]$. Strikingly, freely varying the bulk areas, one finds that the deficit angles $\epsilon_t = 2\pi - \sum_{\sigma \supset t} \theta_t^\sigma$, which measure curvature, have to vanish [36]. That is, the ARC equations of motion impose flatness.

Extended triangulations are built up by gluing pairs of four-simplices (σ, σ') through a shared tetrahedron τ. Gluing identifies six pairs of length variables but only four pairs of area variables, which explains why the equations of motion for LRC and ARC differ: after gluing, there are generically more triangles than edges in a 4D triangulation and, thus, more area than length variables. Restricting variation of the areas to a constraint surface coming from a consistent length assignment $a_t = A_t(l)$, one recovers the LRC equations of motion.

From this counting, we see that, working with area variables, we miss two matching conditions per bulk tetrahedron. The geometry of a tetrahedron, however, can be uniquely specified by its four areas and two 3D dihedral angles at nonopposite edges (intriguingly, opposite dihedral angles do not suffice). Introducing the 3D dihedral angles $\Phi_e^{\tau,\sigma}(a) = \Phi_e^\tau[L^\sigma(a)]$, thus, we have two constraints per bulk tetrahedron

$$\Phi_{e_i}^{\tau,\sigma}(a) - \Phi_{e_i}^{\tau,\sigma'}(a) \stackrel{!}{=} 0, \quad i = 1, 2, \tag{4}$$

where (e_1, e_2) is a choice of a pair of nonopposite edges in τ. Together with the matched areas, these constraints ensure that the lengths of a shared tetrahedron, as defined by the areas associated to σ and σ', match.

The constraints (4) involve pairs of neighboring simplices. Introducing two 3D dihedral angles $\phi_{e_i}^\tau$ per tetrahedron as additional variables [35], we can formulate alternative constraints, localized on a given four-simplex σ

$$\phi_{e_i}^\tau - \Phi_{e_i}^{\tau,\sigma}(a) \stackrel{!}{=} 0, \quad i = 1, 2. \tag{5}$$

These constraints fix all variables $\phi_{e_i}^\tau$ as functions of the areas and impose the constraints (4). We favor these localized constraints because they preserve the additive factorization of the action (3) and lead to the simplifying product factorization of the path integral below, Eq. (8).

In the quantum theory, areas are encoded using SU(2) representation labels j_t, cf. Eq. (1), which result from identifying triangle normals with angular momentum operators. The 3D dihedral angles are given by the inner product of these normals and can be encoded in the recoupling of two angular momenta. The angles at a pair of nonopposite edges (e_1, e_2) in a tetrahedron τ require different recoupling schemes and, therefore, are noncommutative [39,40] (for a simplified proof see [45])

$$\hbar\{\phi^\tau_{e_1}, \phi^\tau_{e_2}\} = \ell_P^2\gamma\frac{\sin\alpha_v^{t,\tau}}{a_t} = \frac{\sin\alpha_v^{t,\tau}}{(j_t+\frac{1}{2})}, \tag{6}$$

where $\alpha_v^{t,\tau}$ is the angle between (e_1, e_2). Thus, the constraints (5) are also noncommutative, more precisely, second class. For these second class constraints, the uncertainty relations prevent a sharp imposition of the constraints in the quantum theory. Armed with these understandings, we take up the path integral.

Path integral.—To incorporate a discrete area spectrum (1), we employ constrained ARC, and sum over spin labels j_t

$$\mathcal{Z} = \sum_{\{j_t\}}\mu(j)\prod_t\mathcal{A}_t(j)\prod_\sigma\mathcal{A}_\sigma(j)\prod_{\tau\in\mathrm{blk}}G^{\sigma,\sigma'}_\tau(j). \tag{7}$$

The triangle $\mathcal{A}_t = \exp[i\gamma n_t\pi(j_t+\frac{1}{2})]$ and simplex amplitudes $\mathcal{A}_\sigma = \exp[-i\gamma\sum_{t\in\sigma}(j_t+\frac{1}{2})\theta^\sigma_t(j)]$ result from the exponentiated ARC action (3). The precise form of the measure factor $\mu(j)$ will not be important for the discussion here, but see [46]. The factors $G^{\sigma,\sigma'}_\tau$ implement the constraints (4) and are crucial for imposing the dynamics of LRC instead of the flat dynamics of ARC.

However, imposing the constraints (4) sharply, i.e., setting $G^{\sigma,\sigma'}_\tau(j) = 1$ if the constraints are satisfied, and $G^{\sigma,\sigma'}_\tau(j) = 0$, otherwise, leads to a severe problem: as we allow only discrete values for the areas, the constraints (4) constitute diophantine conditions. These conditions can only be satisfied for a very small set of labels with accidental symmetries, e.g., if all ten pairs of labels match [45]. The resulting reduction in the density of states prevents a reasonable quantum dynamics. This obstacle has also been encountered in higher gauge formulations of gravity [47–50].

One way out is to weaken the constraints (4), e.g., by allowing a certain error interval. But, one has to navigate between Scylla—reducing the density of states too much—and Charybdis—imposing a dynamics that does not match GR.

Here, we will take guidance from LQG and impose the constraints as strongly as allowed by the uncertainty relations resulting from (6). To this end, we employ states that are coherent in the two angle variables per tetrahedron but restrict to the eigenspaces for the area operators. There are different constructions available for such states [42,51–53]. For a given tetrahedron τ, we will denote the coherent states $\mathcal{K}_\tau(\phi^\tau_{e_i}; \Phi^{\tau,\sigma}_{e_i})$, where $\phi^\tau_{e_i} = (\phi^\tau_{e_1}, \phi^\tau_{e_2})$ are the arguments of the wave functions, and $\Phi^{\tau,\sigma}_{e_i} = (\Phi^{\tau,\sigma}_{e_1}, \Phi^{\tau,\sigma}_{e_2})$ are the angles on which the wave function is peaked. The coherent states come with a measure $d\mu^\tau_{\mathcal{K}}(\phi_1, \phi_2)$, the precise form of which is immaterial here. These coherent states can be used to define the path integral

$$\mathcal{Z}' = \sum_{\{j_t\}}\mu(j)\int\prod_\tau d\mu^\tau_{\mathcal{K}}(\phi)\prod_t\mathcal{A}_t(j)\prod_\sigma\mathcal{A}'_\sigma(j,\phi), \tag{8}$$

where the new simplex amplitude is given by

$$\mathcal{A}'_\sigma(j,\phi) = \mathcal{A}_\sigma(j)\prod_{\tau\in\sigma}\mathcal{K}_\tau[\phi^\tau_{e_i}; \Phi^{\tau,\sigma}_{e_i}(j)]. \tag{9}$$

Integrating out the angles, we regain—without approximation and modulo boundary contributions [54]—a path integral of the form (7) where the factors $G^{\sigma,\sigma'}_\tau$ are given by inner products between coherent states peaked on the angles in τ induced by the areas of σ and σ', respectively,

$$G^{\sigma,\sigma'}_\tau(j) = \langle\mathcal{K}_\tau[\cdot; \Phi^{\tau,\sigma}_{e_i}(j)]|\mathcal{K}_\tau[\cdot; \Phi^{\tau,\sigma'}_{e_i}(j)]\rangle. \tag{10}$$

By construction, this inner product is peaked on the matching conditions (4) and provides a precise sense in which they are weakly imposed. Imposition of these constraints leads to the brackets (6) and, through them, to our main results (12) and (13). Counting the spin configurations contained in different confidence intervals of the $G^{\sigma,\sigma'}_\tau$ factors suggests that the weak imposition of the area constraints leads to a reasonable number of configurations contributing to the path integral (7), see [45].

On the flatness problem.—We consider a first test case for the dynamics encoded in the path integral (7). We choose a triangulation where we can control the scale for the bulk area variable and the bulk curvature through the boundary data. The complex consists of three four-simplices sharing a single bulk triangle. There are no bulk edges, thus, no bulk variables to sum over in LRC, and the bulk deficit angle is determined by the boundary lengths. Nonetheless, in ARC, there is one bulk variable to sum over, which imposes a vanishing deficit angle for the internal triangle in the unconstrained theory.

The amplitude of the path integral consists of two pieces: (i) an oscillatory phase factor, given by the exponentiated ARC action and (ii) the G factors, which are peaked on the area constraints (4) and decay exponentially. We employ scaling arguments and approximate these factors by Gaussians with deviation,

$$\sigma(\Phi) \sim \sqrt{\sin \alpha_v^{t,\tau} / \left(j_t + \frac{1}{2}\right)}, \tag{11}$$

determined by the Poisson brackets (6).

The semiclassical limit, as usually understood for spin foams, amounts to a large j limit. The reason for this is the linear scaling of the action (3) in the areas and, thus, in the spins j. As the amplitudes include an oscillatory and an exponentially decaying factor, there are two conditions for configurations to contribute [21,55]: (i) the oscillatory phase should be stationary, and (ii) the G factors should be near their maxima. As the oscillatory phase is given by the exponentiated area Regge action, the stationarity condition (i) leads to flatness in the unconstrained model. A similar structure of the amplitudes and, hence, a similar flatness problem [21–27], arises for the Engle-Pereira-Rovelli-Livine (EPRL) and Freidel-Krasnov (FK) spin foam models [12].

In the following, we will perform a more detailed analysis and identify a regime in which curved configurations can dominate. A bound, that has heretofore received little attention, emerges. We distinguish the spin scales set by the boundary, j, and by the bulk, j_{blk}. For the minimal triangulations investigated here $j \sim j_{\mathrm{blk}}$.

Since we are interested in the semiclassical limit, we focus on the classical action and on the exponent of the Gaussian G factors. The small $\hbar$ limit of these exponents is dominated by the classical values, from which our scaling results will follow. From (11), we see that the G factors come with a deviation $\sigma(\Phi) \sim 1/\sqrt{j}$ for the 3D dihedral angle, where we assume that the boundary areas $a \sim \gamma \ell_P^2 j$ have approximately equal values, so that the bulk area scales as $a_{\mathrm{blk}} \sim a$. As angles are dimensionless, their derivatives scale as $\partial\Phi/\partial a_{\mathrm{blk}} \sim 1/a$ and $\partial\epsilon/\partial a_{\mathrm{blk}} \sim 1/a$. Thus, we have $\partial\Phi/\partial j_{\mathrm{blk}} \sim 1/j$ and $\partial\epsilon/\partial j_{\mathrm{blk}} \sim 1/j$, and the deviations of the Gaussian G factors, expressed as functions of bulk spin and deficit angle ϵ, respectively, scale as

$$\begin{aligned} \sigma(j_{\mathrm{blk}}) &\sim \left[\frac{\partial\Phi(j_{\mathrm{blk}})}{\partial j_{\mathrm{blk}}}\right]^{-1} \times \sigma(\Phi) \sim j \times \frac{1}{\sqrt{j}} = \sqrt{j}, \\ \sigma(\epsilon) &\sim \left[\frac{\partial\epsilon(j_{\mathrm{blk}})}{\partial j_{\mathrm{blk}}}\right] \times \sigma(j_{\mathrm{blk}}) \sim \frac{1}{j} \times \sqrt{j} = \frac{1}{\sqrt{j}}. \end{aligned} \tag{12}$$

As the angles are invariant under rescaling, we can choose boundary data that induce a given deficit angle ϵ, and then choose a sufficiently large scale j, so that the $\epsilon = 0$ value is outside the deviation interval. Thus, by going to sufficiently large spins j, the constraint part of the amplitudes can peak sharply on nonvanishing curvatures. Note that the deviations $\sigma(j_{\mathrm{blk}})$ and $\sigma(\epsilon)$, as functions of j, are independent of the spectral-spacing parameter γ.

Although the G factors can be peaked on curved configurations, the relevant summation range for the bulk spin j_{blk} scales with $\sqrt{j}$. The oscillatory phase factor can, therefore, average out the expectation value for the deficit angle, see Fig. 1. To avoid this, we need to make sure the oscillations are sufficiently slow

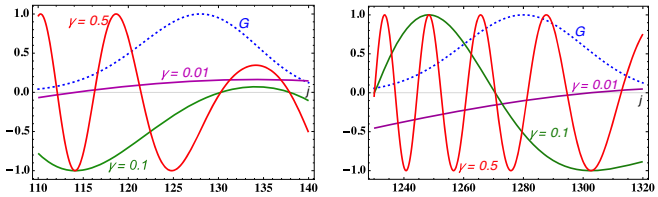

(a) $j = 99.5$ (b) $j = 999.5$

FIG. 1. The G factors (dashed lines), which impose the matching conditions weakly, and the real part of the product of the amplitude factors $\mathcal{A}_t$ and $\mathcal{A}_\sigma$ as functions of the bulk spin j_{blk} for various γ (solid lines) and for an intermediate (a) and a large (b) spin value. Here, the G factors peak on a curvature value $\epsilon \approx 0.5$. Larger γ's lead to a more oscillatory behavior. These examples are detailed in the Supplemental Material [45].

$$\sigma\left(\frac{S_{\mathrm{ARC}}}{\ell_P^2}\right) = \frac{1}{\ell_P^2} \frac{\partial(S_{\mathrm{ARC}})}{\partial j_{\mathrm{blk}}} \times \sigma(j_{\mathrm{blk}}) \sim \gamma\epsilon\sqrt{j} \overset{!}{\lesssim} \mathcal{O}(1). \tag{13}$$

Thus, whereas the scaling for the deficit angle (12) requires a choice of larger j, (13) demands that, with growing j, we choose smaller γ and, thus, a smaller spacing between the area eigenvalues. Taking j large and keeping γ fixed—as for the large j limit discussed above and often treated in the literature—the phase factor will oscillate more and more strongly and suppress the configurations on which the G factors are peaked, see Fig. 1. These expectations are confirmed by numerical examples in the Supplemental Material [45].

We note that γ enters (13) simply because S_{ARC} is linear in the a and $\partial a/\partial j \sim \gamma$ from (1). Depending on which quantity we consider fixed, we can also interpret (13) as a bound on the curvature per triangle $\epsilon \lesssim 1/(\gamma\sqrt{j})$, or a γ- and curvature dependent upper bound on the spin j.

We have considered the simplest triangulation that differentiates between LRC and ARC. As we only employ scaling arguments, similar conclusions may also apply for larger triangulations. In future work, we will investigate examples including bulk edges and vertices. Finally, to reach definite conclusions on the continuum limit, it will be necessary to see how the implementation of the constraints changes under coarse graining. The models proposed here simplify this task immensely.

Discussion.—Area operators are central in a number of approaches to 4D quantum gravity, notably LQG and holography. To achieve a quantum dynamics that reproduces GR, constraints between the areas need to hold. This is, however, hindered if areas have an asymptotically equispaced spectrum and are locally independent.

The imposition of these constraints is pivotal in spin foam quantization. This leads to involved amplitudes,

which, so far, has prevented satisfactory resolution of key dynamical questions, most pressingly, whether the models suppress curvature excitations. Thus, we propose to use, instead of the standard spin foam amplitudes, a class of effective models with a transparent encoding of the dynamics and which are much more amenable for numerical investigations [56,57]. If it becomes clear that these effective models lead to a gravitational dynamics in the large scale limit, one can study the effects of using more involved versions, including a sum over orientations or degenerate geometries [58]. See [59] for first insights in the 3D case.

In the models proposed here, the constraints are imposed weakly, but as strongly as allowed by the LQG Hilbert space, from which the discrete, locally independent area spectra result. Whether this leads to the correct dynamics is not understood, even in much simpler models than gravity, and should be further tested. In particular, for spin foam models, a too weak imposition of the constraints could lead to suppression of curvature.

We have found that curvature is not necessarily suppressed. This result comes with restrictions connecting the average area $a \sim \ell_P^2 \gamma j$, the Barbero-Immirzi parameter γ, and the curvature ϵ_t per triangle. The concentration of the constraints on a given curvature value improves with growing spin j, as $1/\sqrt{j}$, but is independent of γ. Our condition $\gamma\sqrt{j}\epsilon_t \lesssim \mathcal{O}(1)$, prefers small γ and, hence, a small spacing in the area spectrum.

In numerical examples [45], we need large spins and small γ to obtain an expectation value for the deficit angle that well approximates the classical value. This justifies our focus on effective models, where we replace the full spin foam simplex amplitude with its large spin asymptotics, which is already obtained in practice around $j = 10$, and is given by the cosine (replaced here with the exponential) of the Regge action [11,55,60,61].

It has been argued, in [62], that a double scaling limit that takes γ small and spins j large, with γj fixed, reproduces the LRC equations of motion. Here, we also find that γ should be small and j large, but that we need for the combination $\gamma\sqrt{j}\epsilon_t$ to be of order one or smaller. This combination and the related bound on curvature has also been identified in [63], based on a generalized stationary phase analysis of the EPRL-FK amplitudes. Using much simpler inputs, we have shown that this bound does not depend on specific choices for the spin foam amplitudes. Rather, the reason for this bound is tied to the LQG Hilbert space and the area spectrum it leads to.

The conclusions for the expectation value of the curvature hold, in general, but assume that we can control the scale of bulk spin and deficit angles, e.g., via the choice of boundary data. This is not necessarily the case for larger triangulations. To understand the continuum limit, we will have to investigate how these arguments are impacted by coarse graining and renormalization [64]. The investigation of corresponding continuum actions [65], in which the geometricity constraints are also imposed weakly, might elucidate how these constraints behave under renormalization.

The effective model presented here is the numerically fastest spin foam in the literature to date. All the computations for this Letter were performed on individual laptops. The recent work [57], which uses the same triangulation, but works with 4D BF theory was computed on 32-core machines. No comparable computation has been carried out for the full EPRL-FK models [12]. Effective spin foams should make the study of coarse graining flow [64] more feasible than for other spin foam models and will help to establish whether LQG and spin foams allow for a satisfactory continuum limit.

B. D. thanks Wojciech Kaminski, and B. D. and H. M. H. thank Abhay Ashtekar, Eugenio Bianchi, Pietro Donà, Aldo Riello, and Simone Speziale for discussions. S. K. A. is supported by an NSERC grant awarded to B. D. H. M. H. gratefully acknowledges support from the visiting fellows program at the Perimeter Institute and the warm hospitality of the quantum gravity group. Research at Perimeter Institute is supported in part by the Government of Canada through the Department of Innovation, Science and Economic Development Canada and by the Province of Ontario through the Ministry of Colleges and Universities.

*Corresponding author.
hhaggard@bard.edu

[1] G. Ponzano and T. Regge, Semiclassical limit of Racah coefficients, in *Spectroscopic and Group Theoretical Methods in Physics*, edited by F. Bloch (North-Holland Publ. Co., Amsterdam, 1968), pp. 1–58.
[2] H. Waelbroeck and J. A. Zapata, Translation symmetry in $2+1$ Regge calculus, Classical Quantum Gravity **10**, 1923 (1993).
[3] V. Bonzom and B. Dittrich, Dirac's discrete hypersurface deformation algebras, Classical Quantum Gravity **30**, 205013 (2013).
[4] B. Dittrich and P. A. Höhn, From covariant to canonical formulations of discrete gravity, Classical Quantum Gravity **27**, 155001 (2010); Canonical simplicial gravity, Classical Quantum Gravity **29**, 115009 (2012).
[5] A. Ashtekar, New Variables for Classical and Quantum Gravity, Phys. Rev. Lett. **57**, 2244 (1986).
[6] C. Rovelli and L. Smolin, Discreteness of area and volume in quantum gravity, Nucl. Phys. **B442**, 593 (1995); Nucl. Phys. **B456** (1995) 753.
[7] A. Ashtekar and J. Lewandowski, Quantum theory of geometry. 1. Area operators, Classical Quantum Gravity **14**, A55 (1997); Quantum theory of geometry. 2. Volume operators, Adv. Theor. Math. Phys. **1**, 388 (1997).
[8] E. Bianchi and H. M. Haggard, Discreteness of the Volume of Space from Bohr-Sommerfeld Quantization, Phys. Rev. Lett. **107**, 011301 (2011); Bohr-Sommerfeld quantization of space, Phys. Rev. D **86**, 124010 (2012).

[9] W. Wieland, Fock representation of gravitational boundary modes and the discreteness of the area spectrum, Ann. Henri Poincare **18**, 3695 (2017).

[10] A. Perez, The spin foam approach to quantum gravity, Living Rev. Relativity **16**, 3 (2013).

[11] J. W. Barrett and L. Crane, Relativistic spin networks and quantum gravity, J. Math. Phys. (N.Y.) **39**, 3296 (1998).

[12] J. Engle, R. Pereira, and C. Rovelli, The Loop-Quantum-Gravity Vertex-Amplitude, Phys. Rev. Lett. **99**, 161301 (2007); L. Freidel and K. Krasnov, A new spin foam model for 4D gravity, Classical Quantum Gravity **25**, 125018 (2008); E. R. Livine and S. Speziale, Consistently solving the simplicity constraints for spinfoam quantum gravity, Europhys. Lett. **81**, 50004 (2008); J. Engle, E. Livine, R. Pereira, and C. Rovelli, LQG vertex with finite Immirzi parameter, Nucl. Phys. **B799**, 136 (2008); M. Dupuis and E. R. Livine, Holomorphic simplicity constraints for 4D spinfoam models, Classical Quantum Gravity **28**, 215022 (2011); A. Baratin and D. Oriti, Group field theory and simplicial gravity path integrals: A model for Holst-Plebanski gravity, Phys. Rev. D **85**, 044003 (2012).

[13] G. 't Hooft, Dimensional reduction in quantum gravity, Conf. Proc. C **930308**, 284 (1993).

[14] L. Smolin, Four principles for quantum gravity, Fundam. Theor. Phys. **187**, 427 (2017).

[15] S. Ryu and T. Takayanagi, Holographic Derivation of Entanglement Entropy from the Anti-De Sitter Space/Conformal Field Theory Correspondence, Phys. Rev. Lett. **96**, 181602 (2006).

[16] E. Bianchi and R. C. Myers, On the architecture of spacetime geometry, Classical Quantum Gravity **31**, 214002 (2014).

[17] J. D. Bekenstein and V. F. Mukhanov, Spectroscopy of the quantum black hole, Phys. Lett. B **360**, 7 (1995).

[18] A. Ashtekar, J. Baez, A. Corichi, and K. Krasnov, Quantum Geometry and Black Hole Entropy, Phys. Rev. Lett. **80**, 904 (1998).

[19] J. D. Bekenstein, Statistics of black hole radiance and the horizon area spectrum, Phys. Rev. D **91**, 124052 (2015).

[20] J. F. Barbero G. and A. Perez, Quantum geometry and black holes, arXiv:1501.02963.

[21] F. Conrady and L. Freidel, On the semiclassical limit of 4D spin foam models, Phys. Rev. D **78**, 104023 (2008).

[22] V. Bonzom, Spin foam models for quantum gravity from lattice path integrals, Phys. Rev. D **80**, 064028 (2009).

[23] F. Hellmann and W. Kaminski, Holonomy spin foam models: Asymptotic geometry of the partition function, J. High Energy Phys. 10 (**2013**) 165.

[24] M. Han, On spinfoam models in large spin regime, Classical Quantum Gravity **31**, 015004 (2014).

[25] J. R. Oliveira, EPRL/FK asymptotics and the flatness problem, Classical Quantum Gravity **35**, 095003 (2018).

[26] P. Donà, F. Gozzini, and G. Sarno, Searching for classical geometries in spin foam amplitudes: A numerical method, Classical Quantum Gravity **37**, 094002 (2020).

[27] E. Bianchi, J. Engle, and S. Speziale, ILQGS seminar (March 3rd 2020): Panel on the status of the vertex, Slides, http://relativity.phys.lsu.edu/ilqgs/bianchienglespeziale030320.mp4.

[28] A. Barbieri, Quantum tetrahedra and simplicial spin networks, Nucl. Phys. **B518**, 714 (1998); J. C. Baez and J. W. Barrett, The quantum tetrahedron in three-dimensions and four-dimensions, Adv. Theor. Math. Phys. **3**, 815 (1999).

[29] E. Bianchi, P. Donà, and S. Speziale, Polyhedra in loop quantum gravity, Phys. Rev. D **83**, 044035 (2011).

[30] T. Regge, General relativity without coordinates, Nuovo Cim. **19**, 558 (1961).

[31] J. W. Barrett, M. Rocek, and R. M. Williams, A Note on area variables in Regge calculus, Classical Quantum Gravity **16**, 1373 (1999).

[32] R. M. Williams, Recent progress in Regge calculus, Nucl. Phys. B, Proc. Suppl. **57**, 73 (1997); J. Makela, Variation of area variables in Regge calculus, Classical Quantum Gravity **17**, 4991 (2000); J. Makela and R. M. Williams, Constraints on area variables in Regge calculus, Classical Quantum Gravity **18**, L43 (2001).

[33] J. W. Barrett, First order Regge calculus, Classical Quantum Gravity **11**, 2723 (1994).

[34] B. Bahr and B. Dittrich, Regge calculus from a new angle, New J. Phys. **12**, 033010 (2010).

[35] B. Dittrich and S. Speziale, Area-angle variables for general relativity, New J. Phys. **10**, 083006 (2008).

[36] S. K. Asante, B. Dittrich, and H. M. Haggard, The degrees of freedom of area Regge calculus: Dynamics, non-metricity, and broken diffeomorphisms, Classical Quantum Gravity **35**, 135009 (2018).

[37] L. C. Brewin and A. P. Gentle, On the convergence of Regge calculus to general relativity, Classical Quantum Gravity **18**, 517 (2001).

[38] These functions depend on a discrete parameter that accounts for multiple roots appearing in this inversion. This parameter is another summation variable for the (constrained) ARC path integral. To simplify notation, we suppress it here.

[39] B. Dittrich and J. P. Ryan, Phase space descriptions for simplicial 4D geometries, Classical Quantum Gravity **28**, 065006 (2011); Simplicity in simplicial phase space, Phys. Rev. D **82**, 064026 (2010); On the role of the Barbero-Immirzi parameter in discrete quantum gravity, Classical Quantum Gravity **30**, 095015 (2013).

[40] This Poisson bracket (with $\gamma = 1$) appears in the Kapovich-Millson phase space [41], which is used to describe the space of shapes of tetrahedra with fixed areas [8,29,42,43]. The noncommutativity of the angles is inherited by the lengths [39,44].

[41] M. Kapovich and J. J. Millson, The symplectic geometry of polygons in Euclidean space, J. Diff. Geom. **44**, 479 (1996).

[42] F. Conrady and L. Freidel, Quantum geometry from phase space reduction, J. Math. Phys. (N.Y.) **50**, 123510 (2009).

[43] L. Freidel and S. Speziale, Twisted geometries: A geometric parametrization of SU(2) phase space, Phys. Rev. D **82**, 084040 (2010).

[44] E. Bianchi, The length operator in loop quantum gravity, Nucl. Phys. **B807**, 591 (2009).

[45] See Supplemental Material at http://link.aps.org/supplemental/10.1103/PhysRevLett.125.231301 gives a proof of Eq. 6 and details on the numerics referred to throughout the Letter.

[46] B. Bahr, B. Dittrich, and S. Steinhaus, Perfect discretization of reparametrization invariant path integrals, Phys. Rev. D **83**, 105026 (2011); B. Dittrich and S. Steinhaus, Path integral measure and triangulation independence in discrete gravity, Phys. Rev. D **85**, 044032 (2012); B. Dittrich, W. Kaminski, and S. Steinhaus, Discretization independence implies non-locality in 4D discrete quantum gravity, Classical Quantum Gravity **31**, 245009 (2014); B. Bahr and S. Steinhaus, Numerical Evidence for a Phase Transition in 4D Spin Foam Quantum Gravity, Phys. Rev. Lett. **117**, 141302 (2016).

[47] F. Girelli, H. Pfeiffer, and E. M. Popescu, Topological higher gauge theory—from BF to BFCG theory, J. Math. Phys. (N.Y.) **49**, 032503 (2008).

[48] A. Mikovic and M. Vojinovic, Poincare 2-group and quantum gravity, Classical Quantum Gravity **29**, 165003 (2012); M. Vojinovic, Causal dynamical triangulations in the spincube model of quantum gravity, Phys. Rev. D **94**, 024058 (2016).

[49] S. K. Asante, B. Dittrich, F. Girelli, A. Riello, and P. Tsimiklis, Quantum geometry from higher gauge theory, Classical Quantum Gravity **37**, 205001 (2020).

[50] A. Baratin and L. Freidel, Hidden quantum gravity in 4-D Feynman diagrams: Emergence of spin foams, Classical Quantum Gravity **24**, 2027 (2007); A 2-categorical state sum model, J. Math. Phys. (N.Y.) **56**, 011705 (2015).

[51] E. R. Livine and S. Speziale, A new spinfoam vertex for quantum gravity, Phys. Rev. D **76**, 084028 (2007).

[52] V. Bonzom and E. R. Livine, Generating functions for coherent intertwiners, Classical Quantum Gravity **30**, 055018 (2013).

[53] L. Freidel and J. Hnybida, A discrete and coherent basis of intertwiners, Classical Quantum Gravity **31**, 015019 (2014).

[54] These are given by a coherent state $\mathcal{K}_\tau$ for each boundary tetrahedron.

[55] J. W. Barrett and R. M. Williams, The asymptotics of an amplitude for the four simplex, Adv. Theor. Math. Phys. **3**, 209 (1999); J. W. Barrett and C. M. Steele, Asymptotics of relativistic spin networks, Classical Quantum Gravity **20**, 1341 (2003); J. W. Barrett, R. J. Dowdall, W. J. Fairbairn, H. Gomes, and F. Hellmann, Asymptotic analysis of the EPRL four-simplex amplitude, J. Math. Phys. (N.Y.) **50**, 112504 (2009); J. W. Barrett, R. J. Dowdall, W. J. Fairbairn, F. Hellmann, and R. Pereira, Lorentzian spin foam amplitudes: Graphical calculus and asymptotics, Classical Quantum Gravity **27**, 165009 (2010); M. X. Han and M. Zhang, Asymptotics of spinfoam amplitude on simplicial manifold: Euclidean theory, Classical Quantum Gravity **29**, 165004 (2012).

[56] S. Speziale, Boosting Wigner's nj-symbols, J. Math. Phys. **58**, 032501 (2017); P. Donà and G. Sarno, Numerical methods for EPRL spin foam transition amplitudes and Lorentzian recoupling theory, Gen. Relativ. Gravit. **50**, 127 (2018); P. Donà, M. Fanizza, G. Sarno, and S. Speziale, Numerical study of the Lorentzian Engle-Pereira-Rovelli-Livine spin foam amplitude, Phys. Rev. D **100**, 106003 (2019).

[57] P. Donà, F. Gozzini, and G. Sarno, Numerical analysis of spin foam dynamics and the flatness problem, Phys. Rev. D **102**, 106003 (2020).

[58] J. Engle, Proposed proper Engle-Pereira-Rovelli-Livine vertex amplitude, Phys. Rev. D **87**, 084048 (2013); A spin-foam vertex amplitude with the correct semiclassical limit, Phys. Lett. B **724**, 333 (2013).

[59] B. Dittrich, C. Goeller, E. R. Livine, and A. Riello, Quasi-local holographic dualities in non-perturbative 3D quantum gravity I—Convergence of multiple approaches and examples of Ponzano-Regge statistical duals, Nucl. Phys. **B938**, 807 (2019); Quasi-local holographic dualities in non-perturbative 3D quantum gravity II—From coherent quantum boundaries to BMS_3 characters, Nucl. Phys. **B938**, 878 (2019); Quasi-local holographic dualities in non-perturbative 3D quantum gravity, Classical Quantum Gravity **35**, 13LT01 (2018); C. Goeller, E. R. Livine, and A. Riello, Non-perturbative 3D quantum gravity: Quantum boundary states and exact partition function, Gen. Relativ. Gravit. **52**, 24 (2020).

[60] W. Kaminski, M. Kisielowski, and H. Sahlmann, Asymptotic analysis of the EPRL model with timelike tetrahedra, Classical Quantum Gravity **35**, 135012 (2018).

[61] P. Donà, M. Fanizza, G. Sarno, and S. Speziale, SU(2) graph invariants, Regge actions and polytopes, Classical Quantum Gravity **35**, 045011 (2018).

[62] E. Magliaro and C. Perini, Regge gravity from spinfoams, Int. J. Mod. Phys. D **22**, 1350001 (2013); , Emergence of gravity from spinfoams, Europhys. Lett. **95**, 30007 (2011).

[63] M. Han, Semiclassical analysis of spinfoam model with a small Barbero-Immirzi parameter, Phys. Rev. D **88**, 044051 (2013).

[64] B. Bahr and B. Dittrich, Improved and perfect actions in discrete gravity, Phys. Rev. D **80**, 124030 (2009); B. Dittrich, The continuum limit of loop quantum gravity: A framework for solving the theory, arXiv:1409.1450; B. Dittrich, S. Mizera, and S. Steinhaus, Decorated tensor network renormalization for lattice gauge theories and spin foam models, New J. Phys. **18**, 053009 (2016); B. Dittrich and M. Geiller, Flux formulation of loop quantum gravity: Classical framework, Classical Quantum Gravity **32**, 135016 (2015); B. Dittrich, E. Schnetter, C. J. Seth, and S. Steinhaus, Coarse graining flow of spin foam intertwiners, Phys. Rev. D **94**, 124050 (2016); C. Delcamp and B. Dittrich, Towards a phase diagram for spin foams, Classical Quantum Gravity **34**, 225006 (2017); B. Bahr, G. Rabuffo, and S. Steinhaus, Renormalization of symmetry restricted spin foam models with curvature in the asymptotic regime, Phys. Rev. D **98**, 106026 (2018).

[65] K. Krasnov, Gravity as BF theory plus potential, Int. J. Mod. Phys. A **24**, 2776 (2009); Effective metric Lagrangians from an underlying theory with two propagating degrees of freedom, Phys. Rev. D **81**, 084026 (2010).